Inorganic Chemistry

Article

pubs.acs.org/IC

Structurally Diverse Copper(II) Complexes of Polyaza Ligands Containing 1,2,3-Triazoles: Site Selectivity and Magnetic Properties

Pampa M. Guha, Hoa Phan, Jared S. Kinyon, Wendy S. Brotherton, Kesavapillai Sreenath, J. Tyler Simmons, Zhenxing Wang, Ronald J. Clark, Naresh S. Dalal,* Michael Shatruk,* and Lei Zhu*

Department of Chemistry and Biochemistry, Florida State University (FSU), Tallahassee, Florida 32306-4390, United States

Supporting Information

ABSTRACT: Copper(II) acetate mediated coupling reactions between 2,6-bis(azidomethyl)pyridine or 2-picolylazide and two terminal alkynes afford 1,2,3-triazolyl-containing ligands L^1–L^6. These ligands contain various nitrogen-based Lewis basic sites including two different pyridyls, two nitrogen atoms on a 1,2,3-triazolyl ring, and the azido group. A rich structural diversity, which includes mononuclear and dinuclear complexes as well as one-dimensional polymers, was observed in the copper(II) complexes of L^1–L^6. The preference of copper(II) to two common bidentate 1,2,3-triazolyl-containing coordination sites was investigated using isothermal titration calorimetry and, using zinc(II) as a surrogate, in ^{1}H NMR titration experiments. The magnetic interactions between the copper(II) centers in three dinuclear complexes were analyzed via temperature-dependent magnetic susceptibility measurements and high-frequency electron paramagnetic resonance spectroscopy. The observed magnetic superexchange is strongly dependent on the orientation of magnetic orbitals of the copper(II) ions and can be completely turned off if these orbitals are arranged orthogonal to each other. This work demonstrates the versatility of 1,2,3-triazolyl-containing polyaza ligands in forming metal coordination complexes of a rich structural diversity and interesting magnetic properties.

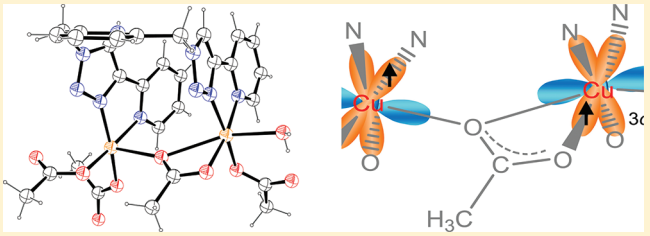

INTRODUCTION

The copper(I)-catalyzed azide–alkyne cycloaddition (CuAAC) reaction provides an important method in molecular conjugation chemistry.[1−4] The heterocyclic 1,2,3-triazolyl ring is known for its large dipole moment (~5 D) and the ability to accept hydrogen bonds, which are beneficial in applications such as drug development[5,6] and the production of peptide mimetics.[7,8] In the past few years, 1,2,3-triazole has also been recognized as a potent hydrogen-bond donor[9] and a metal coordination ligand.[10,11] These discoveries cemented the status of 1,4-disubstituted 1,2,3-triazole as a functionally versatile molecule. In conjunction with the synthetic prowess of the CuAAC reaction, one can anticipate the rapid adoption of 1,2,3-triazolyl as an important functional entity, in addition to a molecular linker, that provides capabilities of hydrogen bonding as both a donor and an acceptor, metal coordination, and π–π interactions in various supramolecular constructs.

Our group is interested in incorporating the 1,2,3-triazolyl group in polydentate ligands for developing fluorescent indicators for metal ions, in particular zinc(II).[12,13] 1,2,3-Triazole has been commonly observed to bind a metal ion via the N3 (N_γ in this paper, Scheme 1) atom.[10] Recently, we[14−16] and others[17−23] have demonstrated the coordination of metal ions by a 1,2,3-triazolyl group via the N2 (N_β in this paper) atom in single-crystal structures. In most reported 1,2,3-triazolyl-containing ligands, a single multidentate binding pocket containing the triazolyl moiety can be readily identified. In the current work, we are curious how 1,2,3-triazolyl participates in metal coordination in a more challenging structural context, in which other ligands compete in binding. Herein, we report our initial findings on the coordination chemistry of 1,2,3-triazolyl-containing ligands that include differently positioned pyridyl and azido functionalities. The paramagnetic copper(II) is the metal ion of choice in this study because of our inherent interest in the magnetic properties of polynuclear copper(II) complexes.[24−28] Structural elucidation of a series of mononuclear, binuclear, and one-dimensional chain structures reveals fascinating effects of the substituents at the 1 and 4 positions of the 1,2,3-triazolyl ring and the counteranions on the coordination mode of 1,2,3-triazole molecules.

Scheme 1. AAC To Afford a 1,2,3-Triazole under Acceleration of $Cu(OAc)_2$[a,15]

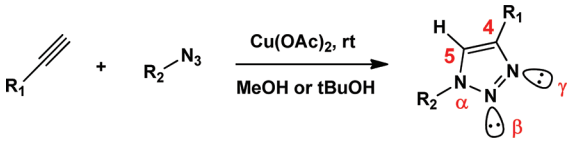

[a]This procedure works particularly well when R_2 is a copper(II) binding ligand, e.g., 2-picolyl group. The numbering of 1,2,3-triazole is shown. We opt to use α, β, and γ, instead of 1, 2, and 3, to number the nitrogen atoms to avoid the confusion in describing the X-ray crystal structures involving 1,2,3-triazoles.

Received: October 4, 2011
Published: March 7, 2012

 © 2012 American Chemical Society dx.doi.org/10.1021/ic2021319 | Inorg. Chem. 2012, 51, 3465–3477

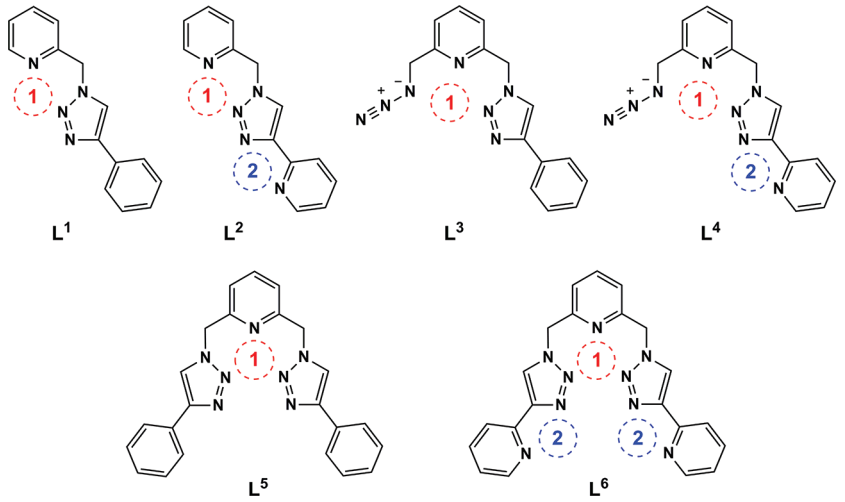

Figure 1. Structures of L^1–L^6. "1" and "2" indicate two binding pockets: a nonplanar pocket involving N_β and a planar one involving N_γ, respectively.

Scheme 2. Reaction Leading to Monotriazolyl (L^3 and L^4) and Ditriazolyl (L^5 and L^6) Ligands[a]

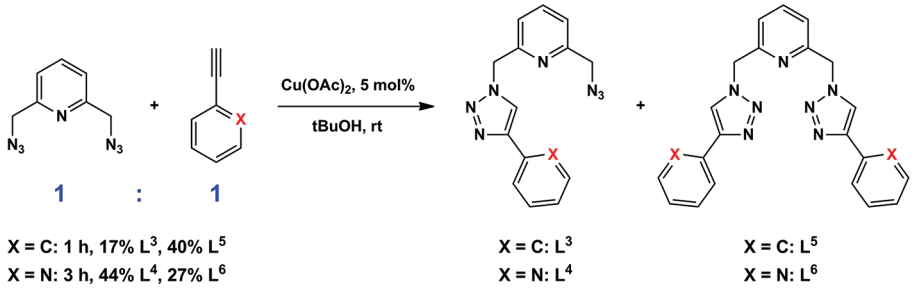

[a]The stoichiometric ratio is 1:1, as shown in blue. Reaction yields are based on the conversion of diazide.

RESULTS AND DISCUSSION

Synthesis. Ligands L^1–L^6 (Figure 1) could be prepared via the typical CuAAC protocols developed by the groups of Fokin/Sharpless and Meldal.[1,2] Our group found that organic azides with a pendant metal coordination ligand (i.e., chelating azides) undergo facile 1,2,3-triazole formation accelerated by $Cu(OAc)_2$ without the addition of a reducing agent (Scheme 1).[29] Incidentally, utilization of chelating azides in the synthesis affords triazolyl-containing multidentate ligands that utilize N_β (pockets 1 in Figure 1), rather than the more Lewis basic N_γ,[30] in 1,2,3-triazolyl in metal chelation.[14,15] This procedure [$Cu(OAc)_2$-AAC; the typical copper(I)-catalyzed reaction is abbreviated as Cu(I)-AAC in this paper] not only increases the rate of the reaction to afford ligands L^1–L^6 but simplifies the purification processes.

Ligands L^1, L^2, L^5, and L^6 were prepared using the $Cu(OAc)_2$-AAC approach, as reported in our previous work.[14,16] These four ligands were also reported by Crowley et al. using a one-pot Cu(I)-AAC reaction.[18,19] Interesting observations were made during the syntheses of monotriazolyl ligands L^3 and L^4 (Scheme 2). Phenylacetylene or 2-ethynylpyridine and 2,6-bis(azidomethyl)pyridine in a 1:1 ratio underwent $Cu(OAc)_2$-AAC reactions upon the slow addition of the alkyne to the diazide. The reaction, judging by consumption of the alkyne component, to produce L^3 was shorter (1 h) than that of L^4 (3 h). However, L^4 was obtained in higher abundance than L^3 (44% vs 17%) when both reactions were performed under the same conditions.

It was reported that when certain diazides take part in Cu(I)-AAC reactions, the ditriazole formation is favored over that of the monotriazole.[31] Similarly, in our case, after formation of the monotriazole L^3 in the reaction involving phenylacetylene, L^3 may hold onto the copper(I) ion in pocket 1 (see Figure 2A) to rapidly turn over the second azido group that is in the proximity. Therefore, monotriazole L^3 is only a minor component (17%) in the product mixture compared to the ditriazole molecule L^5. When 2-ethynylpyridine is used, however, formation of the monotriazole compound L^4 presents a second, thermodynamically more favorable binding pocket for copper (as supported by the X-ray crystal structure of complex **4** in Figure 10). The translocation of the catalytic copper from pocket 1 to pocket 2 (Figure 2B) in L^4 eliminates the coordination of the copper center to the second azido group, thus inhibiting formation of the ditriazole L^6. Consequently, a relatively large abundance of L^4 (44%) was observed in the product mixture. The loss of azido–copper interaction because of the translocation of copper in L^4 also accounts for the longer reaction involving 2-ethynylpridine.

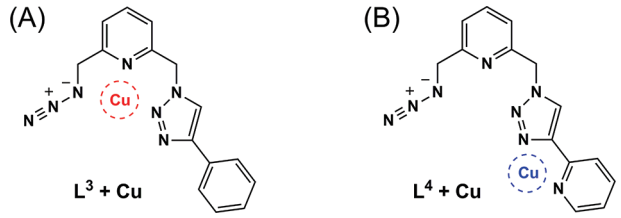

Figure 2. Preferred coordination mode of copper(I/II) to ligands L^3 and L^4.

dx.doi.org/10.1021/ic2021319 | Inorg. Chem. 2012, 51, 3465–3477

Complex $[Cu_2(L^1)_2(OAc)_4]\cdot 4CH_3CN$ (**1**) was prepared by the reaction of $Cu(OAc)_2\cdot H_2O$ and the monotriazole ligand L^1 in CH_3CN. The reaction was first attempted at room temperature, from which only $Cu(OAc)_2\cdot H_2O$ crystallized out after prolonged stirring. Upon heating of the solution up to 45 °C for 4 h, its color changed from blue to dark green, indicating the occurrence of the reaction. Slow evaporation of the CH_3CN solution afforded deep-green single crystals of complex **1**. The ditriazole ligand L^5 did not react with $Cu(OAc)_2$ after prolonged stirring in refluxing CH_3CN. The steric effect due to substitutions at both the 2 and 6 positions of pyridine may have hampered crystallization of the complex. We tried to synthesize the copper(II) complexes with L^3 using perchlorate and chloride as counteranions but failed to obtain single crystals suitable for X-ray diffraction after several trials. The similar reaction with L^4 afforded a few single crystals of complexes $[Cu(L^4)_2(ClO_4)_2]$ (**4**) and $[Cu(L^4)Cl_2]_n$ (**5**), but most of the product was of an oily form. Other copper(II) complexes, $[Cu(L^2)_2(ClO_4)_2]$ (**2**), $[Cu_2(L^2)_2(CH_3CN)_2][Cu_2(L^2)_2(CH_3CN)_4](ClO_4)_8\cdot 2H_2O$ (**3**), $[Cu(L^5)(NO_3)_2]$ (**6**), $[Cu(L^6)_2(H_2O)_2](ClO_4)_2$ (**7**), and $[Cu_2(L^6)(OAc)_4(H_2O)]\cdot 10H_2O$ (**8**), were obtained with high yields and purity from the reactions of respective ligands and copper(II) salts in suitable solvents. All of the complexes were characterized by X-ray crystallography (Table 1), elemental analysis, and UV/vis spectroscopy.

$[Cu_2(L^1)_2(OAc)_4]\cdot 4CH_3CN$ (1). Ligand L^1 has only one bidentate pocket 1 (Figure 1). It has been reported that L^1 forms mononuclear complexes with $Cu(ClO_4)_2$[14] and $CuCl_2$.[18,21] The axial positions of an octahedrally coordinated copper(II) are occupied by an oxygen atom of perchlorate and a nitrogen atom of CH_3CN in complex $[Cu(L^1)(CH_3CN)(ClO_4)](ClO_4)$[14]. The equatorial positions are taken by pyridine nitrogen and N_β of the triazolyl in a bidentate chelation of two L^1 ligands. Structurally similar complexes of L^1 with other metal ions have also appeared in the literature in the past year.[18,21,32−34]

Ligand L^1 upon reacting with $Cu(OAc)_2\cdot H_2O$ displaces the water molecules at axial positions of the dinuclear paddlewheel $[Cu_2(OAc)_4(H_2O)_2]$ and coordinates as a monodentate ligand via pyridyl nitrogen N1 (Figure 3). The triazolyl moiety is not coordinated, which suggests the coordination preference of copper(II) to the pyridyl over the triazolyl. The asymmetric unit of complex **1** consists of an isolated dinuclear complex $[Cu_2(L^1)_2(OAc)_4]$ with the center of symmetry in the midpoint between the two copper(II) centers. The Cu−Cu distance [2.6218(3) Å] and axial Cu−N distance [2.207(1) Å] are typical for axially substituted $[Cu_2(\mu\text{-carboxylate})_4]$ complexes.[35−39] This structure bears resemblance to the complex of L^1 with $Rh(OAc)_2$ recently reported by Košmrlj et al.,[33] where L^1 binds to the dinuclear rhodium(II) paddlewheel at the axial positions.

$[Cu(L^2)_2(ClO_4)_2]$ (2). Ligand L^2 has two binding sites that can form either five- or six-membered rings upon coordination to copper(II), involving the N_γ or N_β atom of the 1,2,3-triazolyl (Figure 1), respectively. Complex **2** was obtained from the reaction of $Cu(ClO_4)_2\cdot 6H_2O$ and L^2 in 2:1 (ligand-to-metal) stoichiometry. It is a mononuclear complex where copper(II) is in an octahedral environment (Figure 4). Two bidentate L^2 ligands occupy the basal plane where Cu−N2 (N_γ) is slightly shorter than Cu−N1 (N_{py}). The axial positions are occupied by perchlorate oxygen atoms with Cu−O1 at 2.419(1) Å. The two L^2 ligands are in a trans configuration. Copper(II) shows a preference to the planar, five-membered chelation pocket 2 over the nonplanar, six-membered pocket 1.

$[Cu_2(L^2)_2(CH_3CN)_2][Cu_2(L^2)_2(CH_3CN)_4](ClO_4)_8\cdot 2H_3O$ (3). By reducing the ligand-to-metal ratio from 2:1 to 1:1, copper(II) was found in both pockets in the dinuclear complex **3**. The asymmetric unit shows two discrete dinuclear copper(II) complexes (**3A** and **3B**). In each structure, the two ligands are trans to each other. The central 1,2,3-triazolyl groups bridge two copper(II) ions, which are bound in the five-membered ring pocket of one ligand and the six-membered ring pocket of the other. Complexes **3A** and **3B** differ in the coordination sphere of copper(II). In **3A**, the two copper(II) centers are square-pyramidal, where the axial position of each copper(II) is occupied by a CH_3CN molecule (Figure 5). The copper(II) centers in **3B** are octahedral with two axial CH_3CN molecules on each metal ion (Figure S1 in the Supporting Information). There is a slight difference in the Cu−Cu distance in the two dinuclear units [4.079(1) Å in **3A** and 4.053(2) Å in **3B**]. In both **3A** and **3B**, the six-membered, nonplanar chelate ring adopts a boat conformation, typical of what has been observed in other complexes containing pocket 1.[14,15,18,21]

The structure of dinuclear copper(II) complex **3** is reminiscent of a dinuclear silver(I) complex of L^2 reported by Crowley and Bandeen.[19] In the silver(I) complex, two tetrahedral silver(I) centers take up all eight Lewis basic nitrogen atoms in two L^2 ligands in the same manner as that observed in complex **3**. The triazolyl moiety bridges the two silver(I) centers, which are separated by 4.98 Å. This value is larger than the Cu−Cu distance in **3** (4.05−4.08 Å) because of the larger ionic radius of silver(I). Bridging 1,2,3-triazolyl groups have also been observed in copper(I) complexes where Cu−Cu distances are 3.618[17] and 3.329 Å,[22] respectively. These distances are shorter than the Cu−Cu distance in **3**, which can be attributed to the stronger repulsive electrostatic interactions between two copper(II) ions in **3** than that in the dinuclear copper(I) complexes.

Coordination Chemistry of L^2 in Solution. The coordination chemistry of L^2 in CH_3CN was investigated using ^1H NMR. The zinc(II) ion was chosen as a diamagnetic analogue of copper(II) in the ^1H NMR titration experiment. The peaks in spectrum 1 (Figure 6) were assigned based on the two-dimensional COSY experiment (Figure S2 in the Supporting Information). The color coding scheme is shown in the ChemDraw structure of L^2 in Figure 6, where the protons in red and blue are associated with the coordination pockets 1 and 2, respectively.

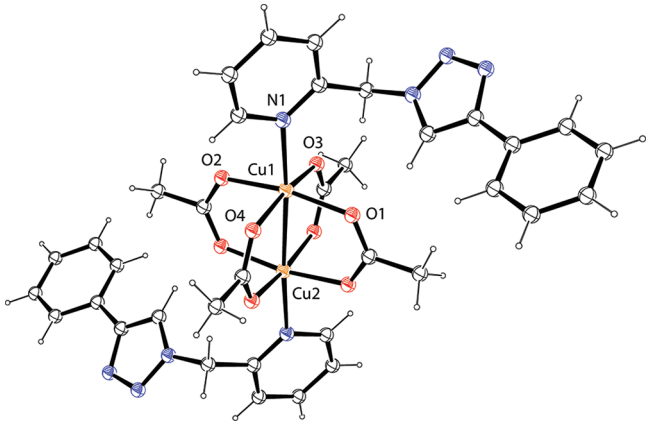

Figure 3. ORTEP view of complex **1**. CH_3CN solvent molecules are omitted for clarity. Thermal ellipsoids are at 50% probability. Selected distances [Å]: N1−Cu1 2.207(1), Cu1−Cu2 2.6218(3).

dx.doi.org/10.1021/ic2021319 | Inorg. Chem. 2012, 51, 3465−3477

Table 1. Crystal Data and Structure Refinement Parameters of Complexes 1−8

	1	2	3	4	5	6	7	8
formula	$C_{44}H_{48}Cu_2N_{12}O_8$	$C_{26}H_{22}Cl_2CuN_{10}O_8$	$C_{64}H_{66}N_{26}O_{34}Cl_8Cu_4$	$C_{28}H_{24}Cl_2CuN_{16}O_8$	$C_{14}H_{12}Cl_2CuN_8$	$C_{23}H_{19}CuN_9O_6$	$C_{42}H_{38}CuN_{18}O_{10}Cl_2$	$C_{29}H_{51}Cu_2N_9O_{19}$
M_r	1000.02	736.98	2281.19	847.07	426.76	581.01	1089.34	956.87
space group	$P2_1/n$	$P2_1/c$	$P2_1/c$	$P\bar{1}$	$P\bar{1}$	$P2_12_12_1$	$P\bar{1}$	$P\bar{1}$
a/Å	13.518(1)	7.7090(8)	12.8536(8)	8.3590(6)	8.834(5)	8.8637(5)	8.169(1)	10.2691(7)
b/Å	7.6783(7)	15.032(2)	17.838(1)	8.3744(6)	9.649(5)	12.7775(7)	12.260(2)	12.8215(9)
c/Å	23.536(2)	12.563(1)	19.007(1)	13.345(1)	10.297(5)	21.231(1)	13.336(2)	16.973(1)
α/deg	90	90	90	98.447(1)	92.974(6)	90	66.806(1)	69.908(1)
β/deg	96.182(1)	91.942(1)	90.832(1)	92.964(1)	105.026(6)	90	80.069(1)	81.982(1)
γ/deg	90	90	90	114.866(1)	101.415(6)	90	72.029(1)	83.833(1)
V/Å^3	2428.7(4)	1455.1(3)	4357.5(5)	831.65(12)	826.0(8)	2404.5(2)	1165.8(3)	2074.0(2)
Z	2	2	2	1	2	4	1	2
d_{calcd}/g·cm^{-3}	1.367	1.682	1.736	1.691	1.716	1.605	1.552	1.532
μ(Mo Kα)/mm^{-1}	0.938	1.004	1.310	0.895	1.661	0.969	0.662	1.111
θ range (deg)	1.8−27.1	2.1−27.1	2.0−25.2	2.7−27.1	2.2−27.4	1.9−25.7	1.9−26.4	2.0−27.1
R_{int}	0.031	0.026	0.045	0.014	0.030	0.052	0.022	0.033
total reflns	25 573	15 949	39 440	9248	5938	18 837	11 391	20 716
unique reflns	5348	3189	7781	3647	3345	4559	4725	9030
data with $I > 2\sigma(I)$	4769	2807	6241	3490	2697	3916	3840	6937
R1 [$I > 2\sigma(I)$]	0.030	0.028	0.061	0.027	0.044	0.039	0.035	0.038
wR2	0.076	0.077	0.200	0.070	0.114	0.085	0.082	0.090
GOF on F^2	0.982	1.048	1.458	0.999	1.034	1.045	0.973	1.040

dx.doi.org/10.1021/ic2021319 | Inorg. Chem. 2012, 51, 3465−3477

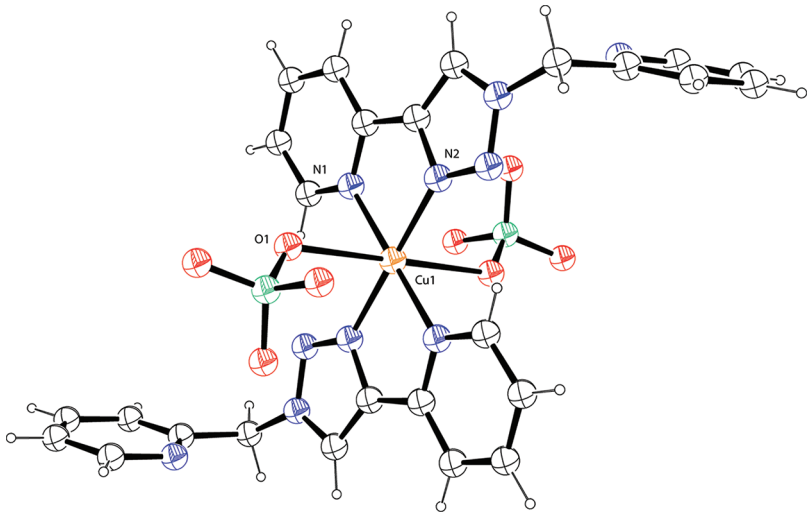

Figure 4. ORTEP view of complex **2**. Thermal ellipsoids are at 50% probability. Selected distances [Å]: N1−Cu1 2.038(1), N2−Cu1 2.027(1), O1−Cu1 2.419(1).

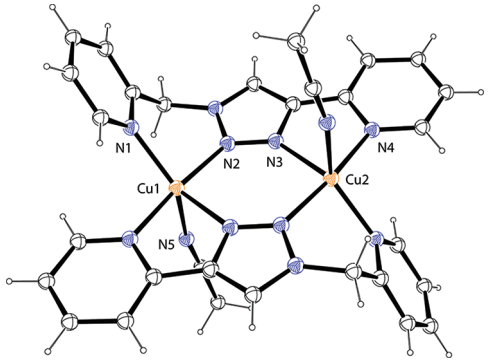

Figure 5. ORTEP view of **3A**. Thermal ellipsoids are at 50% probability. Selected distances [Å]: N1−Cu1 2.004(4), N2−Cu1 1.997(4), N3−Cu2 2.037(4), N4−Cu2 2.003(4), N5−Cu1 2.146(5), Cu1−Cu2 4.079(1).

Upon the initial addition of $Zn(ClO_4)_2$, the hydrogen atoms from the 2-picolyl component (red in Figure 6), which is included in pocket 1, retain their splitting patterns while the pyridyl hydrogen atoms in pocket 2 (blue) show significant shifting and broadening (spectrum 2). As the zinc(II) addition continues, the broadened signals reemerge in spectrum 3, where the peaks that undergo the most changes are the protons of pocket 2 (e.g., H_F and H_I). H_E, which is the methylene hydrogen in pocket 1, shows no change at this point nor do H_B and H_D. Further addition of zinc(II) leads to a downfield shift of H_E and the separation of H_B and H_D, indicating the occupation of pocket 1 by zinc(II). All other peaks undergo slight downfield shifts, as anticipated in a metal coordination process. The two-step sequential binding is the most obvious when the shift of H_A (green triangles in Figure 6) is followed. The solution coordination behavior of $\mathbf{L}^2$ mirrors the observations in the solid state where the preferred coordination site for copper(II) and zinc(II) is pocket 2. Pocket 1 can be filled at high metal-ion concentrations.

Investigators of 1,2,3-triazole coordination chemistry have invoked the higher Lewis basicity of N_γ than that of N_β to explain the observed favorability of N_γ in metal coordination.[23,30] We examined the thermodynamic origin of the formation of copper(II) complexes at pockets 2 and 1 separately using isomeric ligands $\mathbf{L}^1$ and $\mathbf{L}^7$ (Figure 7). Ligand $\mathbf{L}^1$ forms 2:1 (ligand-to-metal) complexes with copper(II).[14,18,21] In this work, ligand $\mathbf{L}^7$ also predictably forms a 2:1 (ligand-to-metal) complex with $Cu(ClO_4)_2$ (Figure 8). The planar bidentate sites of two $\mathbf{L}^7$ ligands constitute the square plane of a copper(II)-centered octahedron. The two perchlorate ions are loosely situated at the axial positions. The observed bidentate binding mode of $\mathbf{L}^7$ is similar to the reported $\mathbf{L}^7$ complexes with ruthenium(II),[40] rhenium(I),[41] and silver(I).[18]

The thermodynamics of $\mathbf{L}^1$ and $\mathbf{L}^7$ binding to $Cu(ClO_4)_2$ was studied using isothermal titration calorimetry (ITC), which lately has been applied in small-molecule/metal-coordination systems.[13,42−46] Exothermic binding was observed as $Cu(ClO_4)_2$ was titrated into the CH_3CN solution of ligand $\mathbf{L}^1$ or $\mathbf{L}^7$ (Figure 9). In each case, a major transition occurs at 0.5 mol equiv of the titrant, indicating the formation of a 2:1 (ligand-to-metal) complex, which is consistent with the reported solid-state structures of such complexes.[14,18] There are minor transitions in the case of ligand $\mathbf{L}^7$ that precede the major change at 0.5 mol equiv (Figure 9A), which suggests the formation of a 3:1 (ligand-to-metal) complex. This transition was not analyzed quantitatively in this report because of its small magnitude. Because of the presence of the preceding minor thermal transition, the thermodynamic parameters of $Cu(ClO_4)_2$/$\mathbf{L}^7$ complex formation need to be considered as "estimated". Consequently, the level of accuracy for the set of data pertaining to $\mathbf{L}^7$ is lower than that pertaining to ligand $\mathbf{L}^1$.

The one-site binding model provided in the software by MicroCal was used to fit the titration traces to obtain the association constant per binding site (K) and enthalpy ($\Delta H°$), from which the association entropy ($T\Delta S°$) was calculated.[47] In the fitting process, the copper(II) ion is considered as a "receptor" capable of binding two ligands at identical sites in a 2:1 (ligand-to-receptor) molar ratio. The thermodynamic parameters of the association of copper(II) to a single ligand site are reported (Figure 9). The affinity (K) of the five-membered ring planar pocket 2 (ligand $\mathbf{L}^7$) is ∼100-fold higher than that of the six-membered ring nonplanar pocket 1 (ligand $\mathbf{L}^1$), which is consistent with the observations in the solid state and in the ^1H NMR titration experiment (Figure 6).

The separation of the enthalpic and entropic contributions to the affinity sheds more light on the binding process. The formation enthalpy of the $\mathbf{L}^7$/copper(II) complex is 5.6 kcal·mol^{-1}

dx.doi.org/10.1021/ic2021319 | Inorg. Chem. 2012, 51, 3465−3477

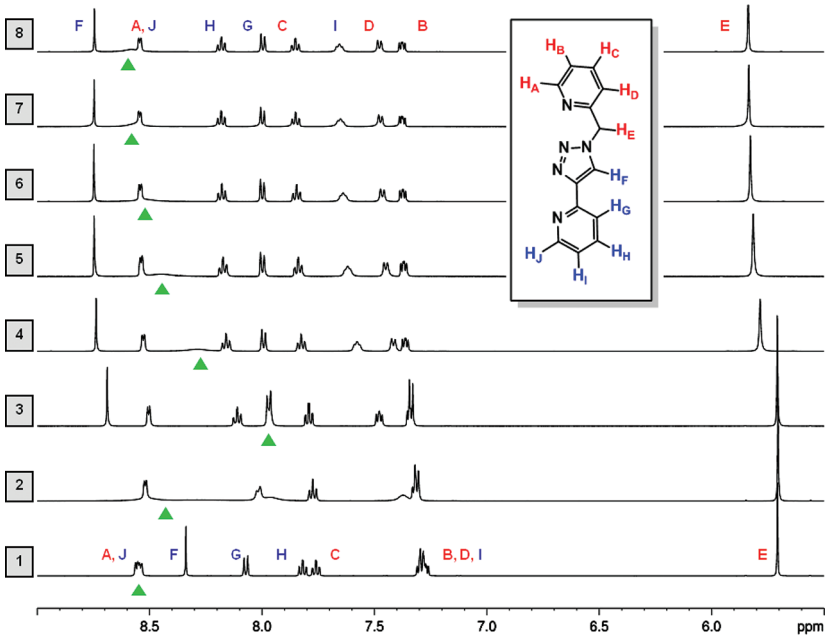

Figure 6. ^{1}H NMR spectra (500 MHz, CD_3CN) of compound $\mathbf{L^2}$ in the presence of increasing concentrations of $Zn(ClO_4)_2$. Spectra 1–8: $[Zn^{2+}]/[\mathbf{L^2}]$ = 0, 0.15, 0.30, 0.45, 0.60, 0.75, 0.90, and 1.06. Green triangles represent the evolution of H_A.

$\mathbf{L^7}$ $\mathbf{L^1}$

Figure 7. Structures of isomeric ligands $\mathbf{L^1}$ and $\mathbf{L^7}$ used in ITC studies.

more favorable than that of the $\mathbf{L^1}$/copper(II) complex. This observation is consistent with the argument that N_γ involved in pocket 2 in $\mathbf{L^7}$ is more Lewis basic than N_β in pocket 1 in $\mathbf{L^1}$. However, the favorable enthalpy of the $\mathbf{L^7}$/copper(II) complex formation is diminished by ~50% because of a more severe entropic penalty than the process involving $\mathbf{L^1}$. The opposite contributions of enthalpy and entropy to the overall affinity can be considered as a form of "enthalpy–entropy compensation", as is often observed in small-molecule host–guest association processes.[48]

$[Cu(L^4)_2(ClO_4)_2]$ (4). Ligand $\mathbf{L^4}$ contains five different nitrogen atoms capable of coordination: two different pyridyl nitrogen atoms (N_{P1} in pocket 1 and N_{P2} in pocket 2), N_β and N_γ of the 1,2,3-triazolyl, and the alkylated nitrogen atom of the azido group (N_Z). All three possible bidentate binding patterns—N_{P1}/N_β,[14] N_{P1}/N_Z,[14] and N_{P2}/N_γ (this work, Figure 8)—have been verified in the copper(II) complexes of the respective bidentate ligands. Ligand $\mathbf{L^4}$ upon reacting with $Cu(ClO_4)_2$ affords mononuclear complex **4** (Figure S3 in the Supporting Information) where copper(II) locates in pocket 2 of $\mathbf{L^4}$ in a five-membered ring chelate similar to that of complex $[Cu(\mathbf{L^7})_2(ClO_4)_2]$ (Figure 8). The unconjugated pyridyl and azido groups are left unbound. Once again, the five-membered chelation pocket 2 shows a higher affinity to copper(II) than the six-membered chelation pocket 1.

$[Cu(L^4)Cl_2]_\eta$ (5). Same as in complex **4**, ligand $\mathbf{L^4}$ upon reacting with $CuCl_2{\cdot}2H_2O$ shows a consistent coordination preference to pocket 2 to result in complex **5** (Figure 10). Ligand $\mathbf{L^4}$ and one of the chlorides act as bridging ligands to provide a six-coordinate environment for the copper(II) ion and to afford a one-dimensional coordination polymer that propagates along the crystallographic *c* axis (Figure 11). The axial positions of the copper(II) center are occupied by a bridging chloride [Cu–Cl = 2.946(2) Å] and an azido group [Cu–N = 2.568(3) Å], while the equatorial plane is formed by

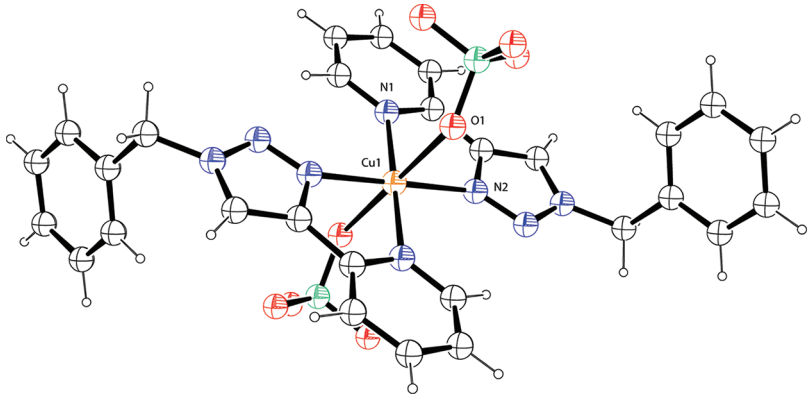

Figure 8. ORTEP view of complex $[Cu(\mathbf{L^7})_2(ClO_4)_2]$. Thermal ellipsoids are at 50% probability. Selected distances [Å]: Cu1–N1 (N_{py}) 2.035(2), Cu1–N2 (N_γ) 2.011(2), Cu1–O1 2.429(2).

dx.doi.org/10.1021/ic2021319 | *Inorg. Chem.* 2012, 51, 3465–3477

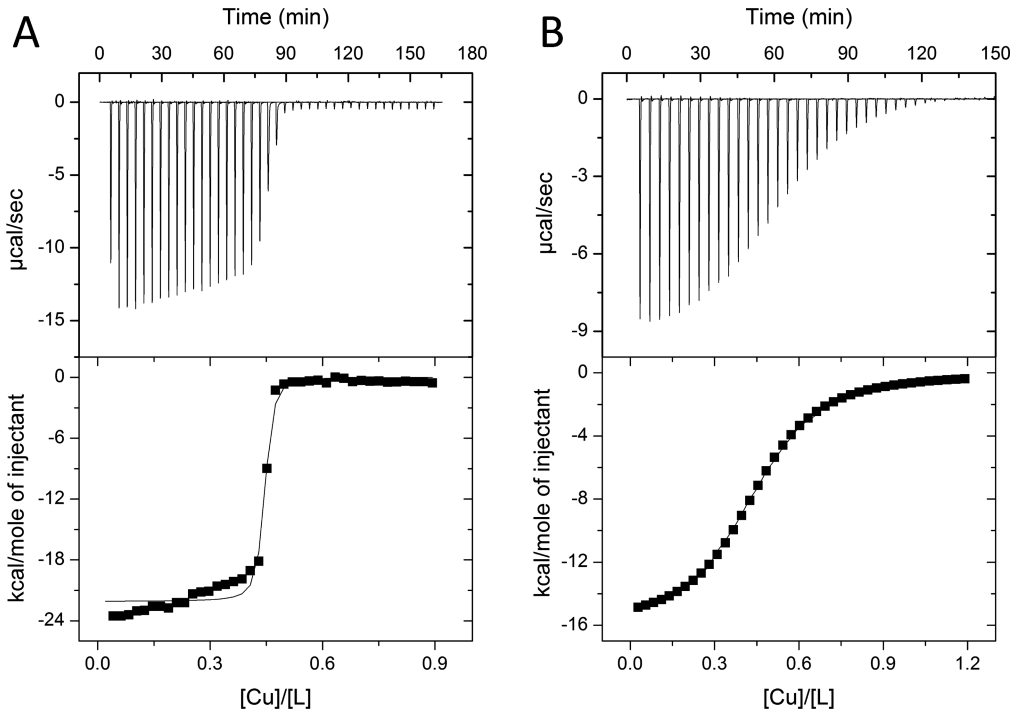

Figure 9. ITC data: (A) a solution of $Cu(ClO_4)_2$ (2.0 mM) is titrated into a solution of ligand $\mathbf{L}^7$ (0.4 mM) in CH_3CN at 298 K. The one-site model was used to fit the data. n (molar ratio) = 0.42 ± 0.04, K = (1.00 ± 0.14) × 10^7 M^{-1} (per binding site), $\Delta H°$ = −(22.0 ± 0.1) kcal·mol^{-1}, and $T\Delta S°$ = −12.5 kcal·mol^{-1}; (B) a solution of $Cu(ClO_4)_2$ (2.0 mM) is titrated into a solution of ligand $\mathbf{L}^1$ (0.3 mM) in CH_3CN at 298 K. The one-site model was used to fit the data. n (molar ratio) = 0.48 ± 0.03, K = (1.01 ± 0.06) × 10^5 M^{-1} (per site), $\Delta H°$ = −(16.4 ± 0.7) kcal·mol^{-1}, and $T\Delta S°$ = −9.5 kcal·mol^{-1}.

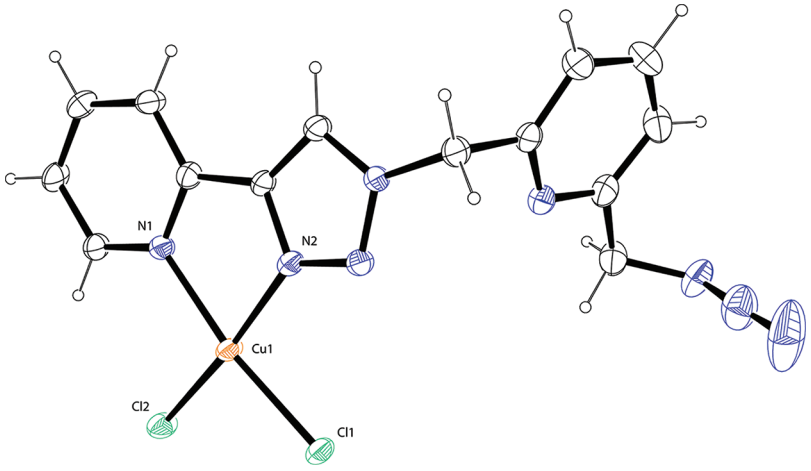

Figure 10. ORTEP view of complex **5**. Thermal ellipsoids are at 50% probability. Selected distances [Å]: Cu1−N1 (N_{py}) 2.057(3), Cu1−N2 (N_γ) 2.022(3), Cu1−Cl1 2.247(1), Cu1−Cl2 2.271(1).

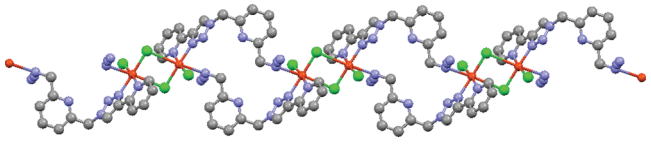

Figure 11. Perspective view of the one-dimensional polymeric chain structure of complex **5**. Cu−Cu distance in one dinuclear core: 3.841(1) Å.

pocket 2, a bridging chloride, and a terminal chloride. The Cu−Cu distance in each dinuclear copper(II) unit is 3.841(1) Å.

$[Cu(L^5)(NO_3)_2]$ (6). Our group previously reported that the tridentate $\mathbf{L}^5$ upon reacting with $Cu(ClO_4)_2$ and $CuCl_2$ gave mononuclear compounds where copper(II) takes the only coordination pocket 1 (Figure 1).[16] A 2:1 (ligand-to-metal) complex containing an octahedral copper(II) forms in the case of a perchlorate salt, whereas $CuCl_2$ leads to a 1:1 complex containing a trigonal-bipyramidal copper(II). $Cu(NO_3)_2·H_2O$ also forms a 1:1 complex with $\mathbf{L}^5$ but with a different copper(II) geometry. The asymmetric unit consists of a copper(II) center that is octahedrally coordinated by a pyridyl nitrogen atom (N1), two triazolyl N_β atoms (N2 and N3), and two nitrate anions (Figure S4 in the Supporting Information). One nitrate anion is bidentate and coordinates copper(II) through atoms O1 and O2, whereas the other nitrate is monodentate.

dx.doi.org/10.1021/ic2021319 | Inorg. Chem. 2012, 51, 3465−3477

$[Cu(L^6)_2(H_2O)_2](ClO_4)_2$ (7). Ligand L^6 contains one tridentate nonplanar coordination pocket 1 and two bidentate planar pockets 2. Similar to complexes **2**, **4**, and **5**, the five-membered chelate pocket 2 of L^6 is preferred by the copper(II) ion. $Cu(ClO_4)_2 \cdot 6H_2O$ upon reacting with L^6 affords a mononuclear complex **7** with a ligand-to-metal ratio at 2:1 (Figure S5 in the Supporting Information). Copper(II) occupies one of the two pockets 2 in L^6, leaving the other two binding sites vacant. Two water molecules coordinate at the axial positions of the copper(II) ion. The noncoordinating component of the ligand curves over the apical water ligand where a hydrogen bond between the water ligand and the free conjugated pyridyl is observed [d(O1···N3) = 2.797(3) Å].

$[Cu_2(L^6)(OAc)_4 \cdot H_2O] \cdot 10H_2O$ (8). Ligand L^6 upon reacting with $Cu(OAc)_2 \cdot H_2O$ affords a completely different complex (**8**; Figure 12). The asymmetric unit includes two copper(II) ions

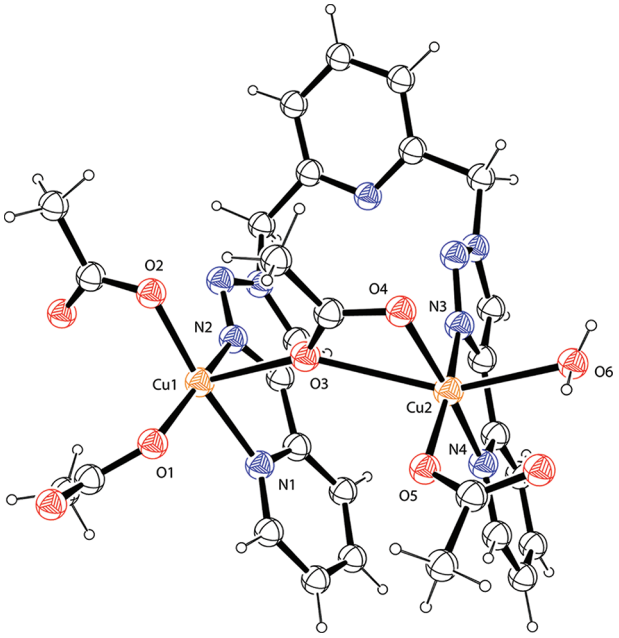

Figure 12. ORTEP view of complex **8**. The 10 noncoordinating water molecules are omitted for clarity. The thermal ellipsoids are at 50% probability. Selected distances [Å]: Cu1–O1 1.941(2), Cu1–O2 1.939(2), Cu1–O3 2.316(2), Cu1–N1 2.062(2), Cu1–N2 1.993(2), Cu2–O3 2.643(2), Cu2–O4 1.970(2), Cu2–O5 1.950(2), Cu2–O6 2.334(2), Cu2–N3 1.985(2), Cu2–N4 2.024(2), Cu1–Cu2 4.701(1).

in two pockets 2 of the same ligand, leaving pocket 1 unbound. The two copper(II) centers are not equivalent. Cu1 is in a square-pyramidal environment where N_γ of triazolyl (N2), N1 of pyridyl, and O1 and O2 from two monodentate acetates constitute the square plane. O3 from the bridging acetate takes the apical position. On the other side, Cu2 is in an octahedron whose square plane consists of the same set of donor atoms in the other pocket 2 [N_γ of triazole (N3) and N4 of pyridyl], O5 of a monodentate acetate, and O4 from the bridging acetate. O6 of a water molecule and O3 of the bridging acetate occupy the axial positions. It should be noted that the Cu2–O3 distance [2.643(2) Å] is relatively long, which may or may not qualify as a coordinative bond.[49] The four acetate anions are not coordinatively equivalent. Three of them are monodentate anions, and the last one acts as a monodentate ligand toward Cu1 and a bidentate ligand toward Cu2, thus bridging the two copper(II) centers through O3 (Figure 12).

Magnetic Properties of Dinuclear Complexes 1, 3, 5, and 8. The magnetic properties of dinuclear copper(II) complexes **1**, **3**, **5**, and **8** were studied by means of SQUID magnetometry on polycrystalline samples and electron paramagnetic resonance (EPR) spectroscopy on pellet samples (to avoid partial alignment in the high magnetic field). For complex **1**, the χT value at 320 K is 0.44 emu·K·mol^{-1}, which is smaller than the spin-only value of 0.75 emu·K·mol^{-1} expected for two noninteracting $S = {}^1/_2$ copper(II) ions. Upon lowering the temperature, χT decreases rapidly and nearly linearly to a value only slightly above 0 and remains essentially constant below 70 K (Figure 13A). The observed behavior indicates a strong antiferromagnetic superexchange between the copper(II) ions, which is in agreement with the well-established behavior of paddlewheel-type dicopper(II) tetraacetate complexes.[50–52] The superexchange can be described by the Heisenberg–Dirac–van Vleck Hamiltonian

$$\hat{H} = -2J\hat{S}_1 \cdot \hat{S}_2 \tag{1}$$

where J is the magnetic exchange coupling constant and S_1 and S_2 are the interacting spin states. This leads to the Bleaney–Bowers equation,[53] which describes the temperature dependence of χT:

$$\chi T = \frac{2Ng^2\mu_B{}^2}{k} \frac{1}{3 + \exp(-2J/kT)} + (\chi T)_{imp} \tag{2}$$

where the second term was introduced to account for the presence of a small amount of mononuclear copper(II) paramagnetic impurity and to achieve a satisfactory fit at low temperatures. The best fit to the experimental data was obtained with an isotropic g factor of 2.05, the magnetic exchange constant $J = -161$ cm^{-1}, and 0.9 mol % paramagnetic impurity ($R^2 = 0.9973$).

As follows from the obtained best-fit parameters, the $S = 0$ ground state appears at 322 cm^{-1} ($-2J$) below the $S = 1$ excited state. High-frequency EPR (HFEPR) measurements were used to obtain the magnetic parameters of the excited state, i.e., the g values and zero-field-splitting parameters D and E.[53] The EPR spectrum of **1** recorded at 275 GHz and 300 K reveals a pattern characteristic of a zero-field split $S = 1$ spin state with a uniaxial **g** tensor (Figure 14, top). The spectrum was simulated with $g_x = g_y = 2.0665(5)$, $g_z = 2.3650(5)$, $D = 0.345$ cm^{-1}, and $E = 0$. The axial symmetry of the **g** tensor is consistent with the nearly tetragonal local symmetry of the copper(II) ions in the crystal structure of **1** (Figure 3). The zero-field splitting D can be expressed as the sum of the exchange and dipolar components (D_{ex} and D_{dip}):

$$D = D_{ex} + D_{dip} \tag{3}$$

$$D_{ex} = \frac{1}{8}J\left[\frac{1}{4}(g_z{}^2 - 2) - (g_x - 2)^2\right] \tag{4}$$

$$D_{dip} = \frac{-(2g_z{}^2 + g_\perp{}^2)\beta^2}{2r^3} \tag{5}$$

Inserting the experimentally determined J and g values in eqs 3–5 yields the calculated D value of 0.40 cm^{-1} ($D_{ex} = 0.58$ cm^{-1}; $D_{dip} = -0.18$ cm^{-1}), which is in agreement with the measured value of 0.345 cm^{-1}.

The magnetic behavior of **3** is similar to that of **1**, although the decrease in χT with the temperature is slower (Figure 13B), indicating a weaker antiferromagnetic superexchange via the 1,2,3-triazolyl bridges in **3** relative to that via the carboxylate bridge in **1**. Indeed, fitting the experimental data to eq 2

dx.doi.org/10.1021/ic2021319 | Inorg. Chem. 2012, 51, 3465–3477

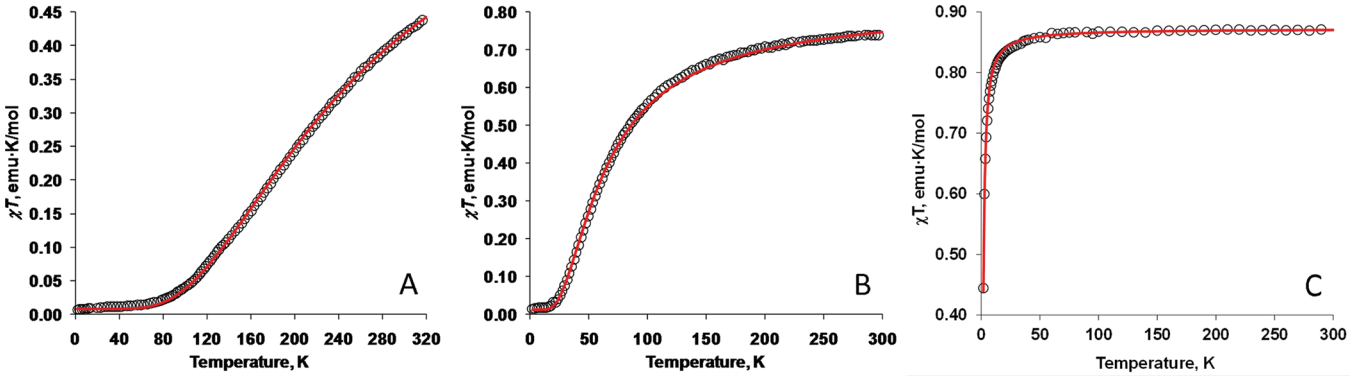

Figure 13. Temperature dependences of χT for complexes **1** (A), **3** (B), and **5** (C). The red solid lines represent the best fit to the experimental data (circles) using the Bleaney–Bowers equation (2). See the text for the best-fit parameters.

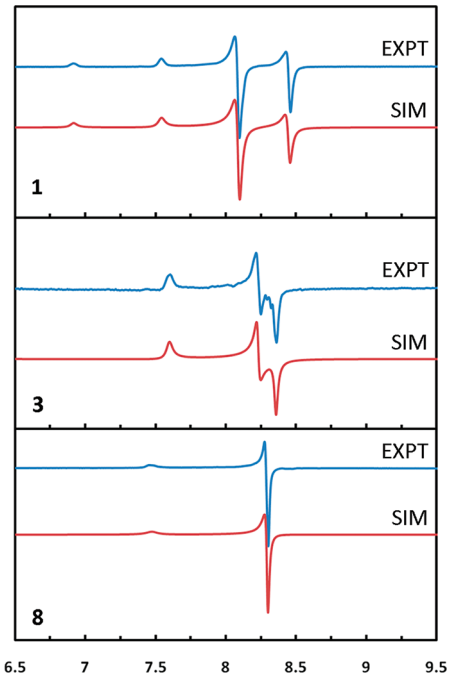

Figure 14. Experimental (EXPT, cornflower) EPR spectra of **1**, **3**, and **8** recorded at 275 GHz and 300 K and their theoretical simulations (SIM, garnet).

resulted in the best-fit parameters of g = 2.09, J = −39 cm^{-1}, and 1.5% mononuclear copper(II) impurity (R^2 = 0.9938). Note that the same J value was used for both dimers present in the crystal structure of **3**, taking into account the similarity of the Cu–N_{bridge} bond lengths, Cu–N_{bridge}–N_{bridge} bond angles, and Cu–Cu distances in these dimers.

The EPR spectrum of **3** does not exhibit a zero-field-splitting pattern (Figure 14, middle) in contrast to **1**. The spectrum was simulated with a rhombic **g** tensor, resulting in g_x = 2.0457(5), g_y = 2.0770(5), and g_z = 2.2502(5). The rhombic symmetry of the **g** tensor is consistent with the lower symmetry of the local coordination environment of the copper(II) ions in the crystal structure of **3**.

The χT value of the chloride-bridged copper(II) dimeric unit of coordination polymer **5** is 0.86 emu·K·mol^{-1} at 300 K, which is higher than the spin-only value of 0.75 emu·K·mol^{-1} expected for two noninteracting copper(II) ions. The deviation is explained by a slight orbital contribution to the total magnetic moment. The χT value remains almost constant down to 45 K and decreases rapidly below this temperature, indicating a weak antiferromagnetic superexchange mediated by the bridging chloride ions (Figure 13C). Fitting the experimental data to the Bleaney–Bowers equation (2) resulted in g = 2.16 and J = −1 cm^{-1}. These values are in line with those of reported bis(μ-chloro)dicopper(II) complexes.[54–56]

Complex **8** exhibits an essentially constant χT value in the 2–300 K temperature range (Figure 15A), indicating negligible magnetic coupling between the copper(II) ions in the dimer. The average value of χT is 0.98 emu·K·mol^{-1}, higher than the spin-only value of 0.75 emu·K·mol^{-1} expected for two noninteracting S = $^1/_2$ copper(II) ions. The deviation is

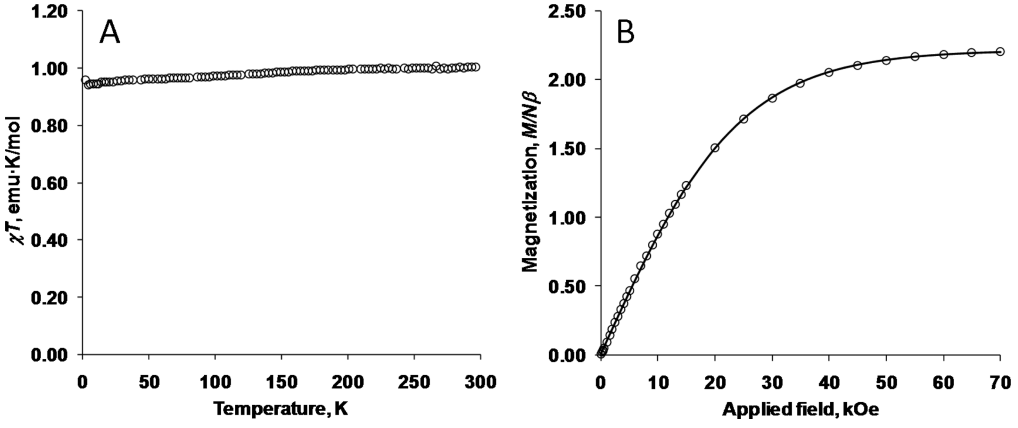

Figure 15. Temperature dependence of χT (A) and field dependence of magnetization at 1.8 K (B) for complex **8**. The solid line represents the best fit to the Brillouin function for two noninteracting copper(II) ions with g_{av} = 2.24.

dx.doi.org/10.1021/ic2021319 | Inorg. Chem. 2012, 51, 3465–3477

explained by a slight orbital contribution to the total magnetic moment. The field-dependent magnetization curve measured at 1.8 K is best fit by the Brillouin function for two noninteracting copper(II) ions with g_{av} = 2.24 (Figure 15B). A satisfactory simulation of the experimental EPR spectrum (Figure 14, bottom) was obtained with a uniaxial **g** tensor: $g_x = g_y$ = 2.0605(5), and g_z = 2.2865(5).

The much weaker magnetic exchange between the copper(II) ions in the monoacetate-bridged dinuclear complex **8**, as compared to the strong coupling observed in tetraacetate-bridged complex **1**, can be attributed to the change in the orbital superexchange pathway. In both complexes, the coordination environment of the copper(II) ion exhibits various extents of axial elongation due to the Jahn–Teller distortion, which leaves the $d_{x^2-y^2}$ orbital directed along the shorter equatorial bonds to act as the magnetic orbital. In complex **1**, this orbital participates in the direct $\sigma-\sigma$ overlaps with acetate ligands involved in the superexchange pathway (Figure 3), thus resulting in the strong magnetic coupling between the copper(II) ions. In contrast, in the structure of **8** (Figure 12), the bridging acetate has a strong $\sigma-\sigma$ overlap only with the $d_{x^2-y^2}$ orbital of the Cu2 center (Figure 16), while the bond to the Cu1 ion is formed through

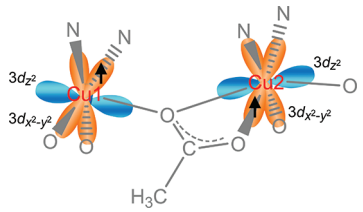

Figure 16. Arrangement of the $d_{x^2-y^2}$ and d_{z^2} orbitals at the copper(II) centers in dinuclear complex **8**. Only the unpaired spins on the magnetic $d_{x^2-y^2}$ orbitals are indicated.

an overlap with the d_{z^2} orbital, leaving the $d_{x^2-y^2}$ orbital of this ion essentially noninteracting (of δ type) with respect to the ligand's orbitals that provide the superexchange pathway. This explains the negligible magnetic coupling between the two acetate-bridged copper(II) ions in complex **8**. These orbital considerations complement other reports on ferromagnetically coupled dinuclear copper(II) complexes.[49,57]

SUMMARY

In coordination with 1,2,3-triazolyl-containing polyaza ligands that include pyridyl and azido groups, copper(II) prefers the five-membered, planar chelation pocket involving pyridyl nitrogen and N_γ in 1,2,3-triazolyl over the six-membered, nonplanar pocket involving an unconjugated pyridyl group and N_β in 1,2,3-triazolyl. ITC suggests that this binding preference is primarily enthalpy-driven, which is offset by a noticeable entropic penalty. Depending on the nature of the counterion, mononuclear, dinuclear, and one-dimensional chain structures result. In addition to enriching the versatile coordination chemistry of 1,4-disubstituted 1,2,3-triazole molecules, we are interested in the magnetic properties of polynuclear copper(II) complexes of the triazolyl-containing ligands. The magnetic properties of three dinuclear complexes, **1**, **3**, and **8**, were investigated and shown to be strongly dependent on the arrangement of the magnetic orbitals at the interacting copper(II) centers. While strong antiferromagnetic superexchange between copper(II) ions is observed for **1** and **3**, orthogonality of one of the magnetic orbitals to the superexchange pathway leads to negligible magnetic coupling in **8**. The reported copper(II) coordination chemistry with ligands $\mathbf{L^1}$–$\mathbf{L^6}$ may extend to other transition-metal ions with similar coordination geometrical preference, as demonstrated in a ^{1}H NMR experiment with zinc(II). The investigations along these lines are ongoing in our laboratories and will be reported in due course.

EXPERIMENTAL SECTION

Materials and General Methods. ***Warning!*** *Low-molecular-weight organic azides and copper(II) perchlorate used in this study are potentially explosive. Appropriate protective measures should always be taken when handling these compounds.* Reagents and solvents were purchased from various commercial sources and used without further purification unless otherwise stated. Analytical thin-layer chromatography (TLC) was performed using precoated TLC plates with silica gel 60 F254 (EMD). Flash-column chromatography was performed using 40–63 μm (230–400 mesh ASTM) silica gel (EMD). ^{1}H NMR spectra were recorded at 300 or 400 MHz, and ^{13}C NMR spectra were collected at 100 or 125 MHz (on a 400 or 500 MHz spectrometer). All chemical shifts were reported in δ units relative to tetramethylsilane. $CDCl_3$ was treated with alumina gel prior to use. Mass spectrometry (MS) spectra (ESI) were obtained on a JEOL AccuTOF spectrometer at the Mass Spectrometry Laboratory at FSU. IR spectra were recorded on a PerkinElmer Spectrum 100 series FT-IR spectrometer, equipped with a Universal ATR sampling accessory. The absorption spectra were recorded on a Varian Cary 100 Bio UV/vis spectrophotometer. Elemental analysis data were collected at Atlantic Microlab, Inc., after samples were vacuum-dried for an extended amount of time (up to 18 h). The magnetic susceptibility measurements were carried out on polycrystalline samples using a superconducting quantum interference device (SQUID) magnetometer (Quantum Design MPMS-XL). The direct-current susceptibility was measured in an applied field of 0.1 T in the 1.8–300 K temperature range. Field-dependent magnetization was obtained at 1.8 K, with the magnetic field varied from 0 to 7 T. The data were corrected for diamagnetic contributions using tabulated constants.[58] The EPR measurements were made at the National High Magnetic Field Laboratory, using the HFEPR spectrometers and procedures described earlier.[59,60] The syntheses of ligands $\mathbf{L^1}$[14] and $\mathbf{L^5}$[16] were reported previously.

Synthesis of $\mathbf{L^2}$. 2-(Azidomethyl)pyridine (0.136 g, 1.0 mmol) and 2-ethynylpyridine (0.120 mL, 1.1 mmol) were dissolved in ^{t}BuOH (2.5 mL). To that solution was added $Cu(OAc)_2{\cdot}H_2O$ (25 μL, 0.4 M in water). After 10 min, the reaction mixture was filtered through a short silica plug with CH_2Cl_2/CH_3OH to afford the pure product as a yellow solid in 98% yield. ^{1}H NMR (300 MHz, $CDCl_3$): δ 8.6 (dd, J = 4.8 and 15.0 Hz, 2H), 8.27 (s, 1H), 8.19 (d, J = 8.4 Hz, 1H), 7.79 (td, J = 1.5 and 7.8 Hz, 1H), 7.70 (td, J = 1.5 and 7.5 Hz, 1H), 7.30–7.22 (m, 3H), 5.74 (s, 2H). ^{13}C NMR (75 MHz, $CDCl_3$): δ 154.4, 150.3, 145.0, 149.5, 148.9, 137.5, 137.0, 123.6, 123.0, 122.9, 122.5, 120.4, 55.9. HRMS ($[M + H]^+$): m/z 238.1093 (calcd), 238.1093 (found).

Syntheses of $\mathbf{L^3}$ and $\mathbf{L^5}$. 2,6-Bis(azidomethyl)pyridine (38 mg, 0.20 mmol) and phenylacetylene (22 μL, 0.20 mmol) were dissolved in CH_3OH (4.0 mL). An aqueous solution of $Cu(OAc)_2{\cdot}H_2O$ (25 μL, 0.4 M, 5 mol %) was added and stirred at room temperature for 1 h. The reaction mixture was then diluted with ethyl acetate and passed through a short plug of silica. Solvent was removed under reduced pressure, and the residue was purified by silica chromatography using a 1:1 hexanes/ethyl acetate mixture. The monotriazole product $\mathbf{L^3}$ was isolated as a viscous oil with 17% (10 mg) yield. ^{1}H NMR (300 MHz, $CDCl_3$): δ 7.97 (s, 1H), 7.83 (d, J = 7.2 Hz, 2H), 7.72 (t, J = 7.8 Hz, 1H), 7.41 (t, J = 7.2 Hz, 2H), 7.28–7.34 (m, 2H), 7.20 (d, J = 7.8 Hz, 1H), 5.70 (s, 2H), 4.45 (s, 2H). ^{13}C NMR (125 MHz, $CDCl_3$): δ 156.3, 154.8, 148.5, 138.6, 130.7, 129.0, 128.4, 125.9, 121.9, 121.8, 120.5, 55.7, 55.4. HRMS-ESI$^+$ ($[M + H^+]$): m/z 292.1311 (calcd), 292.1312 (found). IR (neat)/cm^{-1}: 2097 (azido). The ditriazole product $\mathbf{L^5}$ was isolated as a white solid. Yield: 40% (31 mg). ^{1}H NMR (300 MHz, $CDCl_3$): δ 7.87 (s, 2H), 7.80 (d, J = 7.2 Hz, 4H), 7.71 (t, J = 7.8 Hz, 1H), 7.30–7.42 (m, 6H), 7.20 (d, J = 7.8 Hz, 2H), 5.69 (s, 4H).

dx.doi.org/10.1021/ic2021319 | Inorg. Chem. 2012, 51, 3465–3477

^{13}C NMR (125 MHz, $CDCl_3$): δ 154.8, 148.4, 138.9, 130.5, 129.0, 128.4, 125.8, 122.1, 120.4, 55.4. HRMS (ESI^+, $[M + H^+]$): m/z 394.1780 (calcd), 394.1781 (found).

Syntheses of L^4 and L^6. 2,6-Bis(azidomethyl)pyridine (38 mg, 0.20 mmol) and 2-ethynylpyridine (21 mg, 0.20 mmol) were dissolved in CH_3OH (4.0 mL). An aqueous solution of $Cu(OAc)_2{\cdot}H_2O$ (25 μL, 0.4 M, 5 mol %) was added and stirred at room temperature. After 3 h, the reaction mixture was passed through a short plug of silica. Solvent was removed under reduced pressure, and the residue was purified by silica chromatography using CH_3OH in CH_2Cl_2 (gradient 0−2%). The monotriazole ligand L^4 was isolated as a white solid in 44% (26 mg). ^{1}H NMR (300 MHz, $CDCl_3$): δ 8.56 (d, J = 4.8 Hz, 1H), 8.26 (s, 1H), 8.17 (d, J = 7.8 Hz, 1H), 7.68−7.80 (m, 2H), 7.15−7.32 (m, 3H), 5.72 (s, 2H), 4.47 (s, 2H). ^{13}C NMR (125 MHz, $CDCl_3$): δ 156.4, 154.5, 150.3, 149.6, 149.0, 138.5, 137.1, 123.1, 122.8, 121.8, 121.7, 120.4, 55.8, 55.4. MS-ESI ($[C_{14}H_{12}N_8 + Na]^+$): m/z 315.14 (calcd), 315.10 (found). MS-ESI ($[2L^4 + Na]^+$): m/z 607.0 (calcd), 607.2 (found). IR (neat)/cm^{-1}: 2084 (azido). The ditriazole product L^6 was isolated as a white solid with 27% (22 mg) yield. ^{1}H NMR (300 MHz, $CDCl_3$): δ 8.55 (d, J = 4.8 Hz, 2H), 8.27 (s, 2H), 8.17 (d, J = 7.8 Hz, 2H), 7.79 (t, J = 7.8 Hz, 2H), 7.68 (t, J = 7.8 Hz, 1H), 7.15−7.37 (m, 4H), 5.72 (s, 4H). ^{13}C NMR (125 MHz, $CDCl_3$): δ 154.8, 150.3, 149.6, 149.0, 138.9, 137.1, 123.1, 122.9, 122.1, 120.5, 55.6. HRMS-ESI^+ ($[M + H^+]$): m/z 396.1685 (calcd), 396.1687 (found).

Synthesis of Complex $[Cu_2(L^1)_2(OAc)_4](CH_3CN)_4$ (1). A solution of $Cu(OAc)_2{\cdot}H_2O$ (0.19 g, 1.0 mmol) in CH_3CN (5.0 mL) was added to a solution of ligand L^1 (0.236 g, 1.0 mmol in CH_3CN, 5.0 mL). The resulting mixture was heated to 45 °C and stirred for 4 h. The color of the solution becomes dark green. The solvent was subsequently removed under reduced pressure. The resulting green solid was washed with diethyl ether (3 × 20 mL) to afford the complex in powder form in 78% yield (0.078 g). The product was dissolved in a minimal amount of CH_3CN and filtered through a piece of glass microfiber. Slow evaporation of the CH_3CN solution gave dark-green crystals that were suitable for X-ray diffraction. Anal. Calcd for $C_{36}H_{36}Cu_2N_8O_8$ ($[Cu_2(L^1)_2(OAc)_4]$): C, 51.73; H, 4.34; N, 13.41. Found: C, 52.06; H, 4.37; N, 13.53. λ_{max}/nm (ε_{max}/dm^3·mol^{-1}·cm^{-1}, CH_3CN): 710 (250).

Synthesis of Complex $[Cu(L^2)_2(ClO_4)_2]$ (2). Ligand L^2 (50 mg, 0.21 mmol) was dissolved in CH_3CN (~1 mL). A solution of $Cu(ClO_4)_2{\cdot}6H_2O$ (0.038 g, 0.10 mmol) in CH_3CN (~1 mL) was added dropwise to the ligand solution, and the mixture was stirred for several minutes. The solvent was then removed under reduced pressure, and the complex was rinsed with diethyl ether (3 × 10 mL). The complex was dissolved in a minimal amount of 50:50 CH_3CN/CH_3OH, filtered through a glass microfiber, and set up for vapor diffusion with diethyl ether, which afforded blue X-ray diffraction quality single crystals of **2**. Anal. Calcd for $C_{26}H_{22}Cl_2CuN_{10}O_8$ (**2**): C, 42.37; H, 3.01; N, 19.01. Found: C, 42.59; H, 3.01; N, 19.08. λ_{max}/nm (ε_{max}/dm^3·mol^{-1}·cm^{-1}, CH_3CN): 680 (310).

Synthesis of Complex $[Cu_2(L^2)_2(CH_3CN)_2](ClO_4)_4$ (3A). The ligand L^2 (0.050 g, 0.21 mmol) was dissolved in CH_3CN (~1 mL). A solution of $Cu(ClO_4)_2{\cdot}6H_2O$ (0.077 g, 0.21 mmol) in CH_3CN (~1 mL) was added dropwise to the ligand solution, and the mixture was stirred for several minutes. The solvent was then removed, and the complex was rinsed with diethyl ether (3 × 10 mL). The complex was dissolved in a minimal amount of CH_3CN, filtered through a glass microfiber, and set up for vapor diffusion with diethyl ether. X-ray diffraction analysis reveals two discrete dinuclear copper(II) units (**3A** and **3B**) in an asymmetric unit. The crystals were vacuum-dried before elemental analysis, the result of which matches the composition of structure **3A**. Anal. Calcd for $C_{30}H_{28}Cl_4Cu_2N_{12}O_{16}$ (**3A**): C, 33.32; H, 2.61; N, 15.54. Found: C, 33.43; H, 2.71; N, 15.27. λ_{max}/nm (ε_{max}/dm^3·mol^{-1}·cm^{-1},CH_3CN): 675 (280).

Synthesis of Complex $[Cu(L^4)_2(ClO_4)_2]$ (4). Solutions of ligand L^4 (0.29 g, 1.0 mmol, in 5.0 mL of CH_3OH) and $Cu(ClO_4)_2{\cdot}6H_2O$ (0.37 g, 1.0 mmol, in 5 mL of CH_3OH) were mixed and stirred. The color of the solution became deep blue. The solvent was subsequently removed under reduced pressure. The resulting blue solid was washed with diethyl ether (3 × 20 mL) to afford the complex in 68% yield (0.58 g). The product was dissolved in a minimal amount of CH_3CN and filtered through a piece of glass microfiber. Vapor diffusion of diethyl ether into the blue CH_3CN solution afforded blue X-ray diffraction quality single crystals of **4**. Anal. Calcd for $C_{28}H_{24}Cl_2CuN_{16}O_8$ (**4**): C, 39.70; H, 2.86; N, 26.46. Found: C, 39.84; H, 2.75; N, 26.22. λ_{max}/nm (ε_{max}/dm^3·mol^{-1}·cm^{-1}, CH_3CN): 698 (310).

Synthesis of Complex $[Cu(L^4)Cl_2]_n$ (5). *Method 1.* Complex **5** was obtained by following a procedure similar to that of complex **4**. $CuCl_2{\cdot}2H_2O$ (0.17 g, 1.0 mmol) was used in place of $Cu(ClO_4)_2{\cdot}6H_2O$. A few green single crystals suitable for X-ray diffraction were obtained by vapor diffusion of diethyl ether into a CH_3CN solution of **5**. The isolated yield was low.

Method 2. A CH_3OH (1.0 mL) solution of $CuCl_2{\cdot}2H_2O$ (34 mg, 0.2 mmol) was added to a CH_3OH solution (2.0 mL) of ligand L^4 (58 mg, 0.2 mmol) and stirred for 20 min. The formed pale-green precipitate was washed with CH_3OH (3 × 3.0 mL) and then with diethyl ether (5 × 2.0 mL). It was then dissolved in dimethyl sulfoxide (DMSO; 1.0 mL) and diluted by adding CH_3CN (5.0 mL). The solution was filtered and kept for diethyl ether diffusion, which led to the formation of microcrystals. The crystals were washed with diethyl ether (5 × 2.0 mL) and dried. It was again dissolved in DMSO (1.0 mL) and diluted by adding CH_3OH (20 mL). The solution was filtered and kept for diethyl ether diffusion for overnight. The obtained crystals were verified via X-ray diffraction to be identical with those obtained using method 1. The isolated yield was 44% (37 mg). Anal. Calcd for $C_{14}H_{12}Cl_2CuN_8$ (**5**): C, 39.40; H, 2.83; N, 26.26. Found: C, 39.57; H, 2.81; N, 26.29. λ_{max}/nm (ε_{max}/dm^3·mol^{-1}·cm^{-1}, CH_3CN): 680 (308). IR (neat)/cm^{-1}: 2085 (azido).

Synthesis of Complex $[Cu(L^5)(NO_3)_2]$ (6). Solutions of $Cu(NO_3)_2{\cdot}3H_2O$ (0.19 g, 1.0 mmol in 5.0 mL of CH_3OH) and ligand L^5 (0.30 g, 1.0 mmol in 5.0 mL of CH_3OH) were mixed and stirred. The color of the solution turned to deep blue, and a deep-blue precipitate separated out slowly upon keeping the mixture at room temperature for overnight. The blue solid was then filtered and washed with diethyl ether and redissolved in CH_3OH. Vapor diffusion of diethyl ether into the green solution resulted in the formation of deep-blue single crystals of complex **6**. Yield: 0.46 g, 80%. Anal. Calcd for $C_{23}H_{19}CuN_9O_6$ (**6**): C, 47.55; H, 3.30; N, 21.70. Found: C, 47.81; H, 3.32; N, 21.61. λ_{max}/nm (ε_{max}/dm^3·mol^{-1}·cm^{-1}): 670 (260).

Synthesis of Complex $[Cu(L^6)_2(H_2O)_2](ClO_4)_2$ (7). Solutions of ligand L^6 (0.39 g, 1.0 mmol, in 5.0 mL of CH_3OH) and $Cu(ClO_4)_2{\cdot}6H_2O$ (0.37 g, 1.0 mmol, in 5.0 mL of CH_3OH) were mixed and stirred for 30 min. The color of the solution becomes deep blue. The solvent was subsequently removed under reduced pressure. The resulting blue solid was washed with diethyl ether (3 × 10 mL) to afford the complex in powder form in 76% yield (0.827 g). The product was dissolved in a minimal amount of CH_3OH and filtered through a piece of glass microfiber. Slow evaporation of a CH_3OH solution afforded blue X-ray diffraction quality single crystals of $[Cu(L^6)_2(ClO_4)_2(H_2O)_2]$. Anal. Calcd for $C_{42}H_{38}CuN_{18}O_{10}Cl_2$ ($[Cu(L^6)_2(ClO_4)_2(H_2O)_2]$): C, 46.31; H, 3.52; N, 23.14. Found: C, 46.43; H, 3.59; N, 23.14. λ_{max}/nm (ε_{max}/dm^3·mol^{-1}·cm^{-1}, CH_3CN): 690 (260).

Synthesis of Complex $[Cu_2(L^6)(OAc)_4(H_2O)](H_2O)_{10}$ (8). Complex **8** was obtained by following a procedure similar to that of **7**. $Cu(OAc)_2{\cdot}H_2O$ (0.19 g, 1.0 mmol) was used in place of $Cu(ClO_4)_2{\cdot}6H_2O$. Deep-blue single crystals suitable for X-ray diffraction were obtained by slow evaporation of the CH_3OH solution of **8**. Yield: 0.72 g, 76%. Anal. Calcd for $C_{29}H_{51}Cu_2N_9O_{19}$: C, 36.40; H, 5.37; N, 13.17. Found: C, 36.18; H, 5.03; N, 13.12. λ_{max} (ε_{max}/dm^3·mol^{-1}·cm^{-1}, CH_3CN): 680 (285).

Synthesis of Complex $[Cu(L^7)_2(ClO_4)_2]$. Solutions of ligand L^7 (0.24 g, 1.0 mmol in 5 mL of CH_3CN) and $Cu(ClO_4)_2{\cdot}6H_2O$ (0.37 g, 1.0 mmol in 5 mL of CH_3CN) were mixed and stirred. The color of the solution became deep blue. The solvent was subsequently removed under reduced pressure. The resulting blue solid was washed with diethyl ether (3 × 20 mL) to afford the complex in 79% yield (0.58 g). The product was dissolved in a minimal amount of CH_3CN and filtered through a piece of glass microfiber. Vapor diffusion of CH_2Cl_2 into the blue CH_3CN solution afforded blue X-ray diffraction quality single crystals of $[Cu(L^7)_2(ClO_4)_2]$. Anal. Calcd for $C_{28}H_{24}Cl_2CuN_8O_8$: C,

dx.doi.org/10.1021/ic2021319 | Inorg. Chem. 2012, 51, 3465−3477

45.76; H, 3.29; N, 15.25. Found: C, 45.80; H, 3.22; N, 15.17. λ_{max}/nm (ε_{max}/dm^3·mol^{-1}·cm^{-1}, CH_3CN): 650 (133).

Crystal Data Collection and Refinement. A suitable single crystal was mounted on a goniometer head of a Bruker SMART APEX II diffractometer using a nylon loop with a small amount of Paratone oil (Hampton Research). The crystal was cooled to either −100 or −120 °C in a cold stream of N_2 gas. After a crystal that was indexed to give a satisfactory unit cell was found, a full low-temperature data set was recorded using a sample-to-detector distance of 6 cm. The number of frames taken was typically 2400 using 0.3° ω scans with 20 s of frame collection time. Data integration was performed using the program *SAINT*, which is part of the Bruker suite of programs.[61] Empirical absorption correction was performed using *SADABS*.[62] *XPREP* was used to obtain an indication of the space group, and the structure was solved by direct methods and refined by *SHELXTL*.[63] All non-hydrogen atoms were refined anisotropically, while hydrogen atoms were typically placed in calculated positions and constrained to a riding model. In some cases, the quality of the data was good enough to allow a direct hydrogen assignment.

The nitrogen atoms of CH_3CN in complex **1** have enlarged ellipsoids, which could be modeled as disorder, but this has not been done. In complex **3**, O21 is a lone water molecule. However, none of the Q peaks are appropriate to be assigned as the missing hydrogen atoms. The structure of complex **4** is triclinic-solved as a racemic twin. The ellipsoids of the perchlorate ions present show only a slight sign of disorder. The extreme thinness of the plate of complex **5** is responsible for getting incomplete data, but the data/parameter ratio is still above 10. In complex **8**, the hydrogen atoms of unbound water molecules were refined with the O−H distances restrained using the DFIX command. Because O27 and other water oxygen atoms appear to hydrogen bond to four other oxygen atoms, disordered hydrogen atoms must be present. Thus, at any given instant, the apparent 1.30 Å H−H distance would not really be present. Refining half of the hydrogen atoms seems to push the data too hard.

ITC. Microcalorimetric titrations were carried out using a VP-ITC isothermal titration microcalorimeter (Microcal Inc., Northampton, MA) at 298 K. All solutions were made in spectroscopic-grade CH_3CN. In a typical experiment, the solution (0.4 mM) of a ligand ($\mathbf{L}^1$ or $\mathbf{L}^7$) was placed in a calorimeter cell, and a solution of $Cu(ClO_4)_2$ (2 mM) was taken up in a 250-μL injection syringe. The concentrations of the solutions were adjusted to ensure that the maximum heat change during titration remains within the limit of ±15 μcal·s^{-1} (reference power of the instrument is 15). The syringe was assembled into the chamber for equilibration with stirring at 270 rpm. The chamber temperature (set at 25 °C) usually stabilized within 5 min before the first injection of 6 μL was carried out. A total of 40 injections was programmed at 6 μL each, added over 12 s and spaced 5 min apart. The association enthalpy ($\Delta H°$ in cal·mol^{-1}), stoichiometry or "number of sites" (n), and association constant per binding site (K in M^{-1}) were obtained by fitting the titration data in the *MicroCal Origin Software* package (version 7.0). The association entropy (ΔS in cal·mol^{-1}·K^{-1} or eu) was calculated from fitted values of $\Delta H°$ and K. Each ITC datum was collected by two independent measurements.

^{1}H NMR Titration Procedure. Ligand $\mathbf{L}^2$ (9.1 mg, 0.038 mmol) was dissolved in CD_3CN in a 1-mL volumetric flask to a concentration of 38 mM. This solution (1.0 mL) was added to a screw-cap NMR tube completed with a septum. $Zn(ClO_4)_2·6H_2O$ (108.1 mg, 0.29 mmol) was dissolved with CD_3CN in a 1-mL volumetric flask to a final concentration of 290 mM. The $Zn(ClO_4)_2$ solution was titrated into the NMR tube, and ^{1}H NMR spectra were recorded with a wait time between titrations of 5 min. Eight data points were taken, with the total volume of the addition being 140 μL, which covered the molar ratio ([Zn^{II}]/[$\mathbf{L}^2$]) range from 0 to 1.06.

■ ASSOCIATED CONTENT

Ⓢ Supporting Information

Structures of complexes **3B**, **4**, **6**, and **7** and ^{1}H COSY NMR spectra of ligand $\mathbf{L}^2$. This material is available free of charge via the Internet at http://pubs.acs.org.

■ AUTHOR INFORMATION

Corresponding Author

*E-mail: dalal@chem.fsu.edu (N.S.D.), shatruk@chem.fsu.edu (M.S.), lzhu@chem.fsu.edu (L.Z.).

Notes

The authors declare no competing financial interest.

■ ACKNOWLEDGMENTS

This work was supported by the U.S. National Science Foundation (Grant CHE-0809201 to L.Z. and Grant CHE-0911109 to M.S.). All HFEPR measurements were made at the National High Magnetic Field Laboratory in Tallahassee, FL, which is supported by NSF cooperative Grant DMR-0654118, by the State of Florida, and by the DOE. We are grateful to Dr. Hans van Tol for the help with the EPR measurements. The authors also thank the Institute of Molecular Biophysics at FSU for providing access to a VP-ITC microcalorimeter (Microcal).

■ REFERENCES

(1) Rostovtsev, V. V.; Green, L. G.; Fokin, V. V.; Sharpless, K. B. *Angew. Chem., Int. Ed.* **2002**, *41*, 2596−2599.
(2) Tornøe, C. W.; Christensen, C.; Meldal, M. *J. Org. Chem.* **2002**, *67*, 3057−3064.
(3) Meldal, M.; Tornøe, C. W. *Chem. Rev.* **2008**, *108*, 2952−3015.
(4) Finn, M. G.; Fokin, V. V. *Chem. Soc. Rev.* **2010**, *39*, 1231−1232.
(5) Kolb, H. C.; Sharpless, K. B. *Drug Discovery Today* **2003**, *8*, 1128−1137.
(6) Bourne, Y.; Kolb, H. C.; Radic, Z.; Sharpless, K. B.; Taylor, P.; Marchot, P. *Proc. Natl. Acad. Sci. U.S.A.* **2004**, *101*, 1449−1454.
(7) Horne, W. S.; Yadav, M. K.; Stout, C. D.; Ghadiri, M. R. *J. Am. Chem. Soc.* **2004**, *126*, 15366−15367.
(8) Angelo, N. G.; Arora, P. S. *J. Am. Chem. Soc.* **2005**, *127*, 17134−17135.
(9) Hua, Y.; Flood, A. H. *Chem. Soc. Rev.* **2010**, *39*, 1262−1271.
(10) See many examples in: Struthers, H.; Mindt, T. L.; Schibli, R. *Dalton Trans.* **2010**, *39*, 675−696.
(11) Bai, S.-Q.; Young, D. J.; Hor, T. S. A. *Chem.—Asian J.* **2011**, *6*, 292−304.
(12) Huang, S.; Clark, R. J.; Zhu, L. *Org. Lett.* **2007**, *9*, 4999−5002.
(13) Michaels, H. A.; Murphy, C. S.; Clark, R. J.; Davidson, M. W.; Zhu, L. *Inorg. Chem.* **2010**, *49*, 4278−4287.
(14) Brotherton, W. S.; Michaels, H. A.; Simmons, J. T.; Clark, R. J.; Dalal, N. S.; Zhu, L. *Org. Lett.* **2009**, *11*, 4954−4957.
(15) Kuang, G.-C.; Michaels, H. A.; Simmons, J. T.; Clark, R. J.; Zhu, L. *J. Org. Chem.* **2010**, *75*, 6540−6548.
(16) Brotherton, W. S.; Guha, P. M.; Hoa, P.; Clark, R. J.; Shatruk, M.; Zhu, L. *Dalton Trans.* **2011**, *40*, 3655−3665.
(17) Donnelly, P. S.; Zanatta, S. D.; Zammit, S. C.; White, J. M.; Williams, S. J. *Chem. Commun.* **2008**, 2459−2461.
(18) Crowley, J. D.; Bandeen, P. H.; Hanton, L. R. *Polyhedron* **2010**, *29*, 70−83.
(19) Crowley, J. D.; Bandeen, P. H. *Dalton Trans.* **2010**, *39*, 612−623.
(20) Bai, S.-Q.; Leelasubcharoen, S.; Chen, X.; Koh, L. L.; Zuo, J.-L.; Hor, T. S. A. *Cryst. Growth Des.* **2010**, *10*, 1715−1720.
(21) Urankar, D.; Pinter, B.; Pevec, A.; Rroft, F. D.; Turel, I.; Košmrlj, J. *Inorg. Chem.* **2010**, *49*, 4820−4829.
(22) Manbeck, G. F.; Brennessel, W. W.; Evans, C. M.; Eisenberg, R. *Inorg. Chem.* **2010**, *49*, 2834−2843.
(23) Kilpin, K. J.; Gavey, E. L.; McAdam, C. J.; Anderson, C. B.; Lind, S. J.; Keep, C. C.; Gordon, K. C.; Crowley, J. D. *Inorg. Chem.* **2011**, *50*, 6334−6346.
(24) Kortz, U.; Nellutla, S.; Stowe, A. C.; Dalal, N. S.; van Tol, J.; Bassil, B. S. *Inorg. Chem.* **2004**, *43*, 144−154.
(25) Kortz, U.; Nellutla, S.; Stove, A. C.; Dalal, N. S.; Rauwald, U.; Welnbeck, D.; Ravot, D. *Inorg. Chem.* **2004**, *43*, 2308−2317.

(26) Nellutla, S.; van Tol, J.; Dalal, N. S.; Bi, L.-H.; Kortz, U.; Keita, B.; Nadjo, L.; Khitrov, G.; Marshall, A. G. *Inorg. Chem.* **2005**, 9795−9806.
(27) Mal, S. S.; Basil, B. S.; Ibrahim, M.; Nellutla, S.; van Tol, J.; Dalal, N. S.; Fernandez, J. A.; Lopez, X.; Poblet, R. N.; Bibom, R. N.; Keita, B.; Kortz, U. *Inorg. Chem.* **2009**, *48*, 11636−11645.
(28) Barsukova-Stuckart, M.; Izarova, N. V.; Jameson, G. B.; Ramachandran, V.; Wang, Z.; van Tol, J.; Dalal, N. S.; Biboum, R. N.; Keita, B.; Nadjo, L.; Kortz, U. *Angew. Chem., Int. Ed.* **2011**, *50*, 2639−2642.
(29) Kuang, G.-C.; Guha, P. M.; Brotherton, W. S.; Simmons, J. T.; Stankee, L. A.; Nguyen, B. T.; Clark, R. J.; Zhu, L. *J. Am. Chem. Soc.* **2011**, *133*, 13984−14001.
(30) Bastero, A.; Font, D.; Pericàs, M. A. *J. Org. Chem.* **2007**, *72*, 2460−2468.
(31) Rodionov, V. O.; Fokin, V. V.; Finn, M. G. *Angew. Chem., Int. Ed.* **2005**, *44*, 2210−2215.
(32) Kilpin, K. J.; Crowley, J. D. *Polyhedron* **2010**, *29*, 3111−3117.
(33) Urankar, D.; Pevec, A.; Turel, I.; Košmrlj, J. *Cryst. Growth Des.* **2010**, *10*, 4920−4927.
(34) Bratsos, I.; Urankar, D.; Zangrando, E.; Genova-Kalou, P.; Košmrlj, J.; Alessio, E.; Turel, I. *Dalton Trans.* **2011**, *40*, 5188−5199.
(35) Melnik, M. *Coord. Chem. Rev.* **1982**, *42*, 259−293.
(36) van Niekerk, J. N.; Schoening, F. R. L. *Nature* **1953**, *171*, 36−37.
(37) Tong, M.-L.; Li, W.; Chen, X.-M.; Zheng, S.-L.; Ng, S. W. *Acta Crystallogr., Sect. C* **2002**, *58*, m232−m234.
(38) Lansalot-Matras, C.; Bonnette, F.; Mignard, E.; Lavastre, O. *J. Organomet. Chem.* **2008**, *693*, 393−398.
(39) Meng, L.; Yang, L. Y.; Shi, J. M. *Acta Crystallogr., Sect. E* **2009**, *65*, m646.
(40) Richardson, C.; Fitchett, C. M.; Keene, F. R.; Steel, P. J. *Dalton Trans.* **2008**, 2534−2537.
(41) Obata, M.; Kitamura, A.; Mori, A.; Kameyama, C.; Czaplewska, J. A.; Tanaka, R.; Kinoshita, I.; Kusumoto, T.; Hashimoto, H.; Harada, M.; Mikata, Y.; Funabiki, T.; Yano, S. *Dalton Trans.* **2008**, 3292−3300.
(42) Dobrawa, R.; Lysetska, M.; Ballester, P.; Grune, M.; Würthner, F. *Macromolecules* **2005**, *38*, 1315−1325.
(43) Shunmugam, R.; Gabriel, G. J.; Smith, C. E.; Aamer, K. A.; Tew, G. N. *Chem.—Eur. J.* **2008**, *14*, 3904−3907.
(44) Zhang, L.; Zhu, L. *J. Org. Chem.* **2008**, *73*, 8321−8330.
(45) Younes, A. H.; Zhang, L.; Clark, R. J.; Zhu, L. *J. Org. Chem.* **2009**, *74*, 8761−8772.
(46) Kano, K.; Kondo, M.; Inoue, H.; Kitagishi, H.; Colasson, B.; Reinaud, O. *Inorg. Chem.* **2011**, *50*, 6353−6360.
(47) Ladbury, J. E.; Chowdhry, B. Z. *Biocalorimetry. Applications of Calorimetry in the Biological Sciences*; John Wiley & Sons Ltd.: West Sussex, U.K., 1998.
(48) Anslyn, E. V.; Dougherty, D. A. University Science Books: Sausalito, CA, 2006; Chapter 4, p 216.
(49) Christou, G.; Perlepes, S. P.; Libby, E.; Floting, K.; Huffman, J. C.; Webb, R. J.; Hendrickson, D. N. *Inorg. Chem.* **1990**, *29*, 3657−3666.
(50) Figgis, B. N.; Martin, R. L. *J. Chem. Soc.* **1956**, 3837−3846.
(51) Gregson, A. K.; Martin, R. L.; Mitra, S. *Proc. R. Soc. London A* **1971**, *320*, 473.
(52) Catterick, J.; Thornton, P. *Adv. Inorg. Chem. Radiochem.* **1977**, *20*, 291.
(53) Bleaney, B.; Bowers, K. D. *Proc. R. Soc. London A* **1952**, *214*, 451−465.
(54) Marsh, W. E.; Hatfield, W. E.; Hodgson, D. J. *Inorg. Chem.* **1982**, *21*, 2679−2684.
(55) Marsh, W. E.; Patel, K. C.; Hatfield, W. E.; Hodgson, D. J. *Inorg. Chem.* **1983**, *22*, 511−515.
(56) Bürger, K.-S.; Chaudhuri, P.; Wieghardt, K. *Inorg. Chem.* **1996**, *35*, 2704−2707.
(57) Costa, R.; Moreira, I. d. P. R.; Youngme, S.; Siriwong, K.; Wannarit, N.; Illas, F. *Inorg. Chem.* **2010**, *49*, 285−294.
(58) Bain, G. A.; Berry, J. F. *J. Chem. Educ.* **2008**, *85*, 532−536.
(59) Cage, B.; Hassan, L.; Pardi, L. A.; Krzystek, J.; Brunel, L. C.; Dalal, N. S. *J. Magn. Reson.* **1997**, *124*, 495−498.
(60) Hassan, A. K.; Pardi, L. A.; Krzystek, J.; Sienkiewicz, A.; Goy, P.; Rohrer, M.; Brunel, L. C. *J. Magn. Reson.* **2000**, *142*, 300−312.
(61) *SMART and SAINT*; Bruker AXS Inc.: Madison, WI, 2007.
(62) *SADABS*; Bruker AXS Inc.: Madison, WI, 2001.
(63) Sheldrick, G. M. *Acta Crystallogr., Sect. A* **2008**, *A64*, 112−122.